A Robotic Joint Sensor

Laurence McLean, Lei Chen, William S. P. Robertson
School of Mechanical Engineering
University of Adelaide, Australia
laurence.mclean@adelaide.edu.au

Abstract

This work reports on the current state of a robotic joint sensor unit capable of estimating the relative angular acceleration, velocity and position of hinged robotic links. To this end the accelerometer-only Inertial Measurement Unit (IMU) concept is built upon to incorporate an incremental encoder and extra accelerometer to gather the extra information required to estimate the relative position, velocity and acceleration components. Two cascaded Unscented Kalman Filters are then used to separately estimate the IMU component and the relative component. Simulation of the system shows promising results with all states being estimated under a range of dynamic motions.

1 Introduction

Joint position and velocity data are employed extensively in a variety of robot control systems. In recent times researchers have begun adding additional joint feedback data such as acceleration and jerk into control systems in order to increase machine performance.

Existing methods of obtaining velocity data rely on the often noisy differentiation of positional data from incremental encoders. Due to the noise levels present in the differentiation of sampled encoder data, further differentiation to obtain acceleration yields poor and unusable results [Zhu and Lamarche, 2007]. Observer based systems have been implemented to estimate velocity and acceleration, however these formulations require accurate parameters and mechanical system models that can be difficult to obtain and may vary over time [Petrella *et al.*, 2007]. Numerical methods have also been investigated and successfully applied, however they generally appear to be directed at obtaining velocity data [Su *et al.*, 2005].

With the advent of low-cost MEMs devices research has extended into incorporating such units as gyroscopes and accelerometers into the robotic joint estimation problem. Many approaches have been investigated and range from systems that rely solely on MEMs devices [Cheng and Oelmann, 2010], forgoing encoder units completely, through to formulations that incorporate data from encoders and MEMs gyroscopes and accelerometers that are scattered about the machine [Munoz-Barron *et al.*, 2015].

This work aims to investigate a solution to obtain joint angular position, velocity and acceleration by developing an all-in-one joint sensor unit that can be readily fixed to a robotic joint. To this end an incremental encoder is employed to obtain an estimate of the link's relative position and accelerometers are tasked with obtaining relative angular accelerations and velocities. Sensor fusion techniques are employed to obtain the angular accelerations and velocities from the accelerometers and to then merge this data with the encoder to improve the relative acceleration, velocity and positional estimates. In obtaining the relative joint acceleration and velocity data, this work extends the accelerometer-only IMU concept [Schopp *et al.*, 2010] and as such linear accelerations and angular accelerations and velocities of the robot joint in the inertial frame are also made available.

2 System Model

The modeling of the joint sensor is separated into two sections. First an accelerometer-only IMU attached to a robotic link l_i, is employed to define the linear acceleration of point O in frame B (also attached to link l_i). The angular acceleration and velocity of frame B (Figure 2) in the inertial frame I are also define in this method. The system is then extended by considering the previous link l_{i-1}, upon which frame A is attached. The angular velocity and acceleration of frame A is then obtained via the knowledge that frames A and B are hinged about the common point O. Once the angular velocities and accelerations of frames A and B are known, the summation of angular velocities and accelerations is employed to obtain the relative angular velocity and acceleration

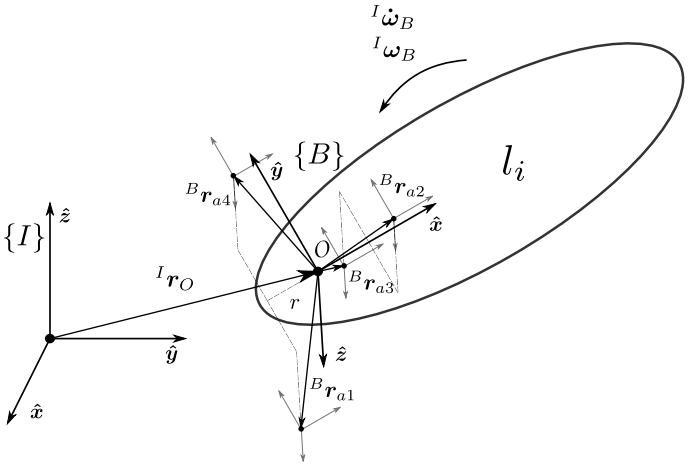

Figure 1: IMU Model.

of frame B with respect to A.

2.1 Accelerometer-Only IMU

The acceleration of a point ${}^I\boldsymbol{a}_{Ai}$ on a rigid body B in inertial frame I is given by

$$ {}^I\boldsymbol{a}_{Ai} = {}^I\boldsymbol{a}_O + {}^I\dot{\boldsymbol{\omega}}_B \times {}^B\boldsymbol{r}_{Ai} + {}^I\boldsymbol{\omega}_B \times ({}^I\boldsymbol{\omega}_B \times {}^B\boldsymbol{r}_{Ai}), \quad (1) $$

with the body B's linear acceleration ${}^I\boldsymbol{a}_O$, angular acceleration ${}^I\dot{\boldsymbol{\omega}}_B$ and the angular velocity ${}^I\boldsymbol{\omega}_B$ being unknown and the known position of point Ai relative to O being given by ${}^B\boldsymbol{r}_{Ai}$.

While there are nine unknown variables required, typically requiring nine equations, it has been shown that as the angular velocity components appear in quadratic form in (1) a minimum of twelve acceleration measurements are required to obtain these nine unknown variables [Lin *et al.*, 2006].

Knowing this four triaxial accelerometers are physically placed on the rigid body B at points ${}^B\boldsymbol{r}_{Ai}$ (Figure 1) and the system of equations is formulated as follows.

For simplicity we let

$$ \begin{aligned} {}^I\boldsymbol{a}_O &= \begin{bmatrix} a_x & a_y & a_z \end{bmatrix}^{\mathrm{T}} \\ {}^I\dot{\boldsymbol{\omega}}_B &= \begin{bmatrix} \dot{w}_x & \dot{w}_y & \dot{w}_z \end{bmatrix}^{\mathrm{T}} \\ {}^I\boldsymbol{\omega}_B &= \begin{bmatrix} w_x & w_y & w_z \end{bmatrix}^{\mathrm{T}} \\ {}^B\boldsymbol{r}_{Ai} &= \begin{bmatrix} r_x & r_y & r_z \end{bmatrix}^{\mathrm{T}}. \end{aligned} \quad (2) $$

The components of (1) are reformulated into the matrix equation

$$ \begin{aligned} {}^I\boldsymbol{a}_{Ai} &= \begin{bmatrix} 1 & 0 & 0 \\ 0 & 1 & 0 \\ 0 & 0 & 1 \\ 0 & -r_z & r_y \\ r_z & 0 & -r_x \\ -r_y & r_x & 0 \\ r_y & r_x & 0 \\ r_z & 0 & r_x \\ 0 & r_z & r_y \\ 0 & -r_y & -r_z \\ -r_x & 0 & -r_z \\ -r_x & -r_y & 0 \end{bmatrix}^{\mathrm{T}} \begin{bmatrix} a_x \\ a_y \\ a_z \\ \dot{w}_x \\ \dot{w}_y \\ \dot{w}_z \\ w_x w_y \\ w_x w_z \\ w_y w_z \\ w_x^2 \\ w_y^2 \\ w_z^2 \end{bmatrix} \\ &= \boldsymbol{B}_i \boldsymbol{x}, \end{aligned} \quad (3) $$

where the known positions are contained in the matrix $\boldsymbol{B}_i$ and the unknown states in the vector $\boldsymbol{x}$. Four such acceleration equations are then stacked as

$$ \boldsymbol{y} = \begin{bmatrix} {}^I\boldsymbol{a}_{A1} & {}^I\boldsymbol{a}_{A2} & {}^I\boldsymbol{a}_{A3} & {}^I\boldsymbol{a}_{A4} \end{bmatrix}^{\mathrm{T}}, \quad (4) $$

which results in a matrix equation of the form

$$ \boldsymbol{y} = \boldsymbol{B}\boldsymbol{x}, \quad (5) $$

where

$$ \boldsymbol{B} = \begin{bmatrix} \boldsymbol{B}_1 & \boldsymbol{B}_2 & \boldsymbol{B}_3 & \boldsymbol{B}_4 \end{bmatrix}^{\mathrm{T}}. \quad (6) $$

Depending on the physical layout of the accelerometers, the unknown states can then be obtained by the inversion of (5).

Equation (5) reveals that obtaining the unknown states depends on the condition of the matrix $\boldsymbol{B}$, which is a function of the accelerometer positions. As such, the condition number of this matrix can serve as an indicator of the quality of the accelerometer placements [Lu and Lin, 2011]. This approach is employed during the determining of the physical placement of the accelerometers and allows for further exploration as to the quality of the expected outputs when investigating sensor placement on different robots.

2.2 Relative Kinematics

The formulation is now extended to obtain estimates of the relative angular acceleration and velocity between frames B and A.

To obtain this information the summation of angular velocities and accelerations is employed and as such requires an estimate of the angular velocity ${}^I\boldsymbol{\omega}_A$ and angular acceleration ${}^I\dot{\boldsymbol{\omega}}_A$ for frame A on link l_{i-1}.

Referring to Figure 2 an accelerometer is placed at ${}^A\boldsymbol{r}_{Aa}$ on frame A with its axes parallel to frame A's axes. As frames A and B are hinged at point O the acceleration of point O can be obtained from the previous IMU estimates with a simple rotation about the $\hat{\boldsymbol{z}}$ axis to

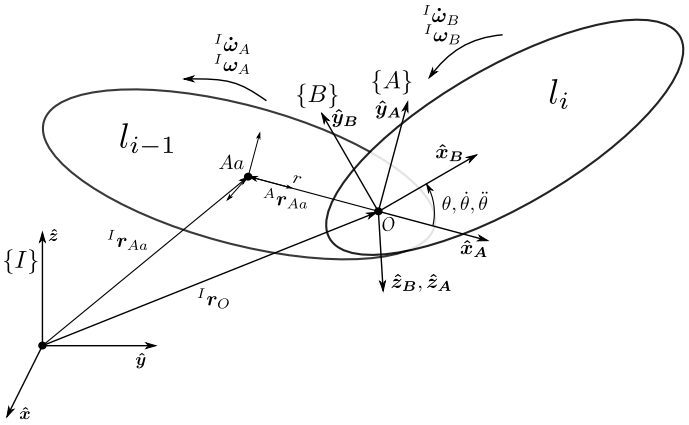

Figure 2: Relative Kinematics Model.

orient it into frame A. The kinematic relationship for acceleration can now be employed to find the angular acceleration and velocity of frame A.

$$^I\boldsymbol{a}_{Aa} = R(\theta)^I\boldsymbol{a}_O + {}^I\dot{\boldsymbol{\omega}}_A \times {}^A\boldsymbol{r}_{Aa} + {}^I\boldsymbol{\omega}_A \times ({}^I\boldsymbol{\omega}_A \times {}^A\boldsymbol{r}_{Aa}) \quad (7)$$

where $R(\theta)$ is the rotation matrix

$$R(\theta) = \begin{bmatrix} \cos(\theta) & -\sin(\theta) & 0 \\ \sin(\theta) & \cos(\theta) & 0 \\ 0 & 0 & 1 \end{bmatrix} \quad (8)$$

and $^I\boldsymbol{\omega}_A$ and $^I\dot{\boldsymbol{\omega}}_A$ are the angular velocity and acceleration of frame A respectively.

To obtain the relative angular velocity and acceleration between the frames the rule of summation of angular velocities and accelerations is employed as

$$\begin{aligned} {}^I\boldsymbol{\omega}_B &= {}^I\boldsymbol{\omega}_A + {}^A\boldsymbol{\omega}_B \\ {}^I\dot{\boldsymbol{\omega}}_B &= {}^I\dot{\boldsymbol{\omega}}_A + {}^A\dot{\boldsymbol{\omega}}_B. \end{aligned} \quad (9)$$

As the joint is hinged about the $\hat{\boldsymbol{z}}$ axis, the values of interest are found as

$$\begin{aligned} {}^A\boldsymbol{\omega}_B &= \dot{\theta}\hat{\boldsymbol{z}} \\ {}^A\dot{\boldsymbol{\omega}}_B &= \ddot{\theta}\hat{\boldsymbol{z}}, \end{aligned} \quad (10)$$

and as such the relative kinematic relationship between the two links is found as

$$\begin{aligned} {}^I\omega_{Ax} &= {}^I\omega_{Bx} & {}^I\dot{\omega}_{Ax} &= {}^I\dot{\omega}_{Bx} \\ {}^I\omega_{Ay} &= {}^I\omega_{By} & {}^I\dot{\omega}_{Ay} &= {}^I\dot{\omega}_{By} \\ {}^I\omega_{Az} &= {}^I\omega_{Bz} - \dot{\theta}\hat{\boldsymbol{z}} & {}^I\dot{\omega}_{Az} &= {}^I\dot{\omega}_{Bz} - \ddot{\theta}\hat{\boldsymbol{z}}. \end{aligned} \quad (11)$$

In this case the $\hat{\boldsymbol{x}}$ and $\hat{\boldsymbol{y}}$ components of frame A's angular acceleration and velocity are equal to frame B's angular acceleration and velocity due to the perceived rigidity in these directions as a result of the hinged joint. The values in frame B are taken from the IMU estimate.

3 Sensor Fusion

The vector $\boldsymbol{x}$ of unknown kinematic quantities in (5) presents the angular velocity components in both quadratic forms and as products of one another. This well-known issue results in sign ambiguity when attempting to extract the angular velocity components. By incorporating the use of Kalman-style filters the angular acceleration components can be merged with the angular velocity components to obtain robust angular velocity measurements. To add to this, an incremental encoder is also employed to improve the estimates of the relative link components and as such a means to incorporate this measurement is required. The Unscented Kalman Filter was selected for the fusion task as it is suited to the estimation of nonlinear functions. The UKF does not approximate the nonlinear function as in the Extended Kalman Filter, rather the probability distribution is approximated and propagated through the nonlinear model. The UKF also suits well to incorporating the relative kinematic components due to the nonlinear rotation matrix present.

For the sake of brevity an in-depth discussion of the UKF is not presented in this paper; rather focus is maintained on system structure, state and measurement models and covariance matrix issues.

Many variations of UKF exist. In this work an assumption of zero mean additive noise is made which allows the use of the additive zero mean UKF formulation [Wan and Van Der Merwe, 2000]. In this method the system state does not need to be augmented with noise variables which reduces the dimension of the state vectors. Instead, the noise source covariances are simply added to the state covariance. This in turn reduces the complexity of the UKF to order $O(n^3)$, for n states, which is important in the hardware execution phase of the project. It is intended that the UKF system executes at a fast update rate on embedded hardware, which may place a limit on the number of states that can be estimated. In light of this it is found that the estimation of the relative components and the IMU components can be split into two separate UKF implementations. As the relative components only depend on measurements from the IMU, but the IMU does not depend on data from the relative component, the system can be split into two separate UKF implementations. This reduces the execution time to order $O(4^3 + 15^3)$ for the split system as opposed to order $O(19^3)$ for a combined UKF formulation.

3.1 IMU UKF

As a robot is undergoing motion, at any time there is a possibility of highly dynamic manoeuvres occurring which may cause abrupt changes in acceleration, particularly in machines that experience unknown contacts with the environment such as walking robots. To add

to this, the overall formulation of the joint sensor incorporates acceleration measurements at each timestep. As such a constant jerk model is employed for the estimation of the sensor states. In this case it is assumed that both the angular and linear jerk terms are constant in between timesteps and any change accounted for through the addition of process noise via the UKF.

The vector $\boldsymbol{x}_{\text{imu}}$ that contains the IMU states to be estimated is given as

$$\boldsymbol{x}_{\text{imu}} = \begin{bmatrix} \dot{\boldsymbol{a}} & \boldsymbol{a} & \ddot{\boldsymbol{\omega}} & \dot{\boldsymbol{\omega}} & \boldsymbol{\omega} \end{bmatrix}^{\text{T}}, \tag{12}$$

where $\boldsymbol{a} = {}^{I}\boldsymbol{a}_{O}$ is the linear acceleration of point $\boldsymbol{O}$ in the inertial frame and $\dot{\boldsymbol{a}}$ is its associated jerk term. $\boldsymbol{\omega} = {}^{I}\boldsymbol{\omega}_{B}$ is an estimation of the angular velocity of the body B in the inertial frame and $\dot{\boldsymbol{\omega}}$ and $\ddot{\boldsymbol{\omega}}$ are the associated angular acceleration and jerk terms.

At each timestep k, for the sample time T_s the state vector is updated by the UKF via the state model

$$\boldsymbol{x}_{\text{imu}_k} = \begin{bmatrix} \ddot{\boldsymbol{a}} \\ \dot{\boldsymbol{a}} + \ddot{\boldsymbol{a}} T_s \\ \ddot{\boldsymbol{\omega}} \\ \dot{\boldsymbol{\omega}} + \ddot{\boldsymbol{\omega}} T_s \\ \boldsymbol{\omega} + \dot{\boldsymbol{\omega}} T_s + \frac{1}{2}\ddot{\boldsymbol{\omega}} T_s^2 \end{bmatrix}_{\text{imu}_{k-1}} + \boldsymbol{v}_{\text{imu}_{k-1}}. \tag{13}$$

In this model the $\boldsymbol{v}_{\text{imu}}$ term accounts for any uncertainty in the linear and angular components, particularly the jerk and angular velocity components which have no sensor directly associated with them. As such $\boldsymbol{v}_{\text{imu}}$ is seen as a tuning parameter for the UKF.

During the UKF update the state prediction as given in (13) is corrected by an observation of the sensors at each timestep k. The observation model $\boldsymbol{y}_{\text{imu}}$ transforms the predicted states into predicted measurements so that they may be compared with actual sensor readings. The observation model for the IMU component is taken directly from (5) and given as

$$\boldsymbol{y}_{\text{imu}_k} = \boldsymbol{B}_{k-1} + \boldsymbol{w}_{\text{imu}_{k-1}}. \tag{14}$$

The observation noise vector $\boldsymbol{w}_{\text{imu}}$ accounts for sensor noise and is derived from the hardware data sheets.

3.2 Relative UKF

The relative component UKF formulation follows the IMU component UKF and adopts a constant jerk model. In this case the relative state vector

$$\boldsymbol{x}_{\text{rel}} = \begin{bmatrix} \dddot{\theta} & \ddot{\theta} & \dot{\theta} & \theta \end{bmatrix}^{\text{T}} \tag{15}$$

is comprised of the relative link angular jerk $\dddot{\theta}$, acceleration $\ddot{\theta}$, velocity $\dot{\theta}$ and relative link position θ.

The state propagation model for the relative component is given as

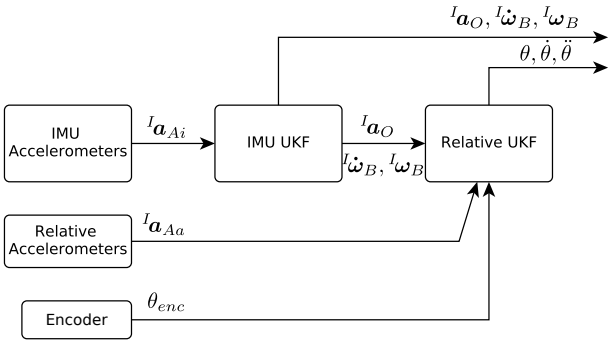

Figure 3: Sensor and UKF Data Flow.

$$\boldsymbol{x}_{\text{rel}_k} = \begin{bmatrix} \dddot{\theta} \\ \ddot{\theta} + \dddot{\theta} T_s \\ \dot{\theta} + \ddot{\theta} T_s + \frac{1}{2}\dddot{\theta} T_s^2 \\ \theta + \dot{\theta} T_s + \frac{1}{2}\ddot{\theta} T_s^2 + \frac{1}{6}\dddot{\theta} T_s^3 \end{bmatrix}_{\text{rel}_{k-1}} + \boldsymbol{v}_{\text{rel}_{k-1}}, \tag{16}$$

again, where T_s is the sample time and $\boldsymbol{v}_{\text{rel}}$ is the process noise that accounts for any uncertainty in the process model and serves as a tuning parameter for the relative UKF component.

As in the IMU component the relative state prediction $\boldsymbol{x}_{\text{rel}_k}$ is corrected by an observation of the sensors. In this case the sensor readings are comprised of a single accelerometer at point ${}^{A}\boldsymbol{r}_{Aa}$ and an incremental encoder that takes the relative angle between frames A and B, and are stacked in the observation vector

$$\boldsymbol{y}_{\text{rel}} = \begin{bmatrix} {}^{I}\boldsymbol{a}_{Aa} & \theta_{\text{enc}} \end{bmatrix}^{\text{T}}. \tag{17}$$

The observation model $\boldsymbol{y}_{\text{rel}_k}$ transforms the predicted relative state $\boldsymbol{x}_{\text{rel}_k}$ into predicted measurements for the accelerometer and encoder, which are then compared with the sensor readings taken during the UKF update.

Expanding (7) and letting ${}^{I}\boldsymbol{a}_{A} = R(\theta){}^{I}\boldsymbol{a}_{O}$ gives the following observation model

$$\boldsymbol{y}_{\text{rel}_k} = \begin{bmatrix} {}^{I}a_{Ax} - r({}^{I}\omega_{Ay}^2 + {}^{I}\omega_{Az}^2) \\ {}^{I}a_{Ay} + r({}^{I}\dot{\omega}_{Az} + {}^{I}\omega_{Ax}{}^{I}\omega_{Ay}) \\ {}^{I}a_{Az} + r({}^{I}\dot{\omega}_{Ay} + {}^{I}\omega_{Ax}{}^{I}\omega_{Az}) \\ \theta_{enc} \end{bmatrix}_{\text{rel}_{k-1}} + \boldsymbol{w}_{\text{rel}_{k-1}}. \tag{18}$$

Again, the observation noise $\boldsymbol{w}_{\text{rel}}$ is assumed Gaussian with values from hardware data sheets.

Figure 3 shows the flow of sensor information and the cascaded UKFs as implemented in simulation.

4 Simulation Results

Simulation results of the joint sensor revolve around the use of a two degree of freedom planar pendulum model

developed in SimMechanics (MathWorks, 2015). The results described in the following simulations are based on a sensor unit as simulated being attached to joint two on the pendulum model. The sensor UKF algorithms are executed at a rate of $T_s = 1\,\text{ms}$ and all initial estimates set to zero. Current results are limited to planar pendulum simulations, however preliminary three dimensional simulations show promising results.

The accelerometer and position sensors themselves are simulated in SimMechanics with sensor noise and other parameters being taken from the device datasheets. For all accelerometers ST Micro LIS3DSH devices are considered with accelerometer signal noise, saturation and digitisation (16 bits as offered by the sensor) being modelled. These sensors have a noise density of $150\,\mu\text{g}/\sqrt{\text{Hz}}$, with a bandwidth of 50 Hz selected. The encoder is a custom device based on an Austria Micro AS5311 device with 18 bit resolution over a full rotation.

The noise density properties of the accelerometers and encoder as taken from the device data sheets are used to build the UKF measurement noise matrix $\boldsymbol{R}$ for both estimators. In obtaining the process noise matrix $\boldsymbol{Q}$ a discrete noise process is assumed, which in turn allows the selection of a variance σ for each process. The noise between the $\hat{\boldsymbol{x}}$, $\hat{\boldsymbol{y}}$ and $\hat{\boldsymbol{z}}$ axes is also assumed independant. A programmed iterative approach to obtaining the best performing σ values for each simulation was adopted. IMU linear (σ_{imulin}) and rotational (σ_{imurot}) values, along with the relative (σ_{relrot}) values are presented in Table 2 for each simulation. Future work will investigate and optimisation approach to obtaining the variance terms.

The performance of the sensor was examined across three simulations of the pendulum with the sensor being attached to joint two to allow examining of the device as it physically moved through space, while sensing the rotation between the two links. Accelerometer placements for the IMU component are such that a rectangular prism is formed with an accelerometer at opposing corners with origin O fixed on the origin of frame B. The placement of the accelerometers is based on dimensions of the hardware platform that the proposed sensor hardware is to be tested on. In this case we take advantage of the length of the robot link and extend the two forward accelerometers up the link length in order to decrease the condition of the matrix $\boldsymbol{B}$ and improve the quality of the sensor output. The placements are given in Equation 19.

$$
\begin{aligned}
{}^{B}\boldsymbol{r}_{A1} &= \begin{bmatrix} -0.015 & -0.026 & 0.026 \end{bmatrix}^{\mathrm{T}} \\
{}^{B}\boldsymbol{r}_{A2} &= \begin{bmatrix} 0.1 & -0.026 & -0.026 \end{bmatrix}^{\mathrm{T}} \\
{}^{B}\boldsymbol{r}_{A3} &= \begin{bmatrix} 0.1 & 0.026 & 0.026 \end{bmatrix}^{\mathrm{T}} \\
{}^{B}\boldsymbol{r}_{A4} &= \begin{bmatrix} -0.015 & 0.026 & -0.026 \end{bmatrix}^{\mathrm{T}},
\end{aligned}
\tag{19}
$$

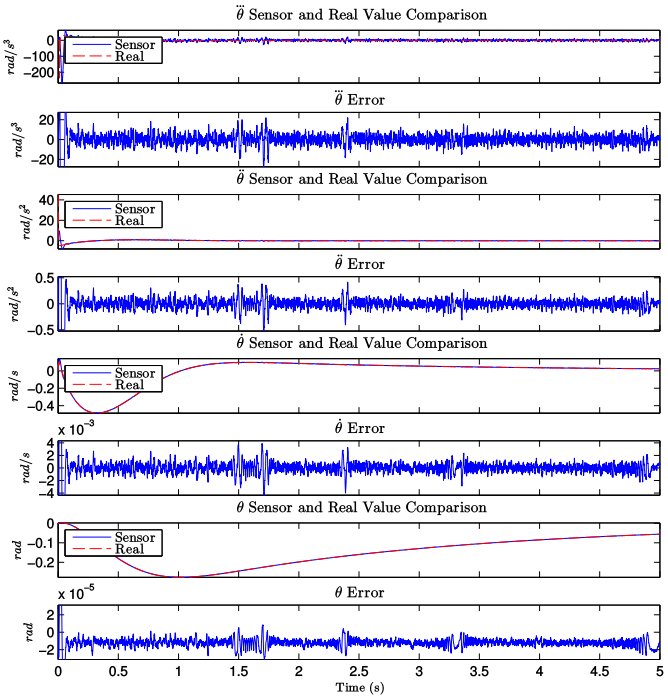

Figure 4: Simulation 1 — Highly Damped: Relative Joint Data.

Similarly, the accelerometer on frame A is placed at ${}^{A}\boldsymbol{r}_{Aa} = [-r, 0, 0]^{\mathrm{T}}$ with $r = 0.06\,\text{m}$.

Simulation−1 examines the sensor's performance on highly damped joints to investigate its performance at low velocities and accelerations. Figure 4 shows the angular jerk, acceleration, velocity and position estimates of the relative component, along with the real values extracted from the simulation. The error terms are also presented. Referring to Figure 4 and Table 1 it is evident that the sensor tracks all components successfully when undergoing slow motions, with the angular jerk and acceleration terms exhibiting more noise than the velocity and position.

Simulation−2 investigates the sensor's performance as the pendulum undergoes low frequency and low amplitude oscillatory motions. This allows examining the peformance of the device under what are deemed typical frequency and amplitude motions that a human or robot may undertake. Again and with reference to Table 1, the simulation shows positive results with the relative position showing an RMS error lower than the maximum resolution of the encoder, however it is evident that the error terms are growing as the motions become more dynamic. Figure 6 shows system convergence from the initial states, with convergence taking about 30 ms.

The output of the sensor as taken from simulation−2 is compared to that of a simple successive derivative and

Table 1: Joint Sensor RMS Error

		Damped	Typical	Chaotic
σ_{imulin}	$\mathrm{m\,s^{-3}}$	10	10	15
σ_{imurot}	$\mathrm{rad\,s^{-3}}$	10	10	70
σ_{relrot}	$\mathrm{rad\,s^{-3}}$	10	10	50
$\dddot{\theta}$	$\mathrm{rad\,s^{-3}}$	4.9805	15.5363	5630.0852
$\ddot{\theta}$	$\mathrm{rad\,s^{-2}}$	0.0879	0.1667	35.1745
$\dot{\theta}$	$\mathrm{rad\,s^{-1}}$	0.0008	1.10×10^{-3}	0.1329
θ	rad	1.27×10^{-5}	1.29×10^{-5}	0.0002
${}^{I}a_{Ox}$	$\mathrm{m\,s^{-2}}$	0.1545	0.1547	0.9081
${}^{I}a_{Oy}$	$\mathrm{m\,s^{-2}}$	0.1542	0.1547	1.7206
${}^{I}a_{Oz}$	$\mathrm{m\,s^{-2}}$	0.1542	0.1542	0.1908
${}^{I}\dot{\omega}_{Bx}$	$\mathrm{rad\,s^{-2}}$	0.0008	0.0053	9.1769
${}^{I}\dot{\omega}_{By}$	$\mathrm{rad\,s^{-2}}$	0.0112	0.0051	2.9407
${}^{I}\dot{\omega}_{Bz}$	$\mathrm{rad\,s^{-2}}$	0.0078	0.2226	17.0427
${}^{I}\omega_{Bx}$	$\mathrm{rad\,s^{-1}}$	0.0102	0.0002	0.2783
${}^{I}\omega_{By}$	$\mathrm{rad\,s^{-1}}$	0.1616	0.0002	0.4004
${}^{I}\omega_{Bz}$	$\mathrm{rad\,s^{-1}}$	0.0116	0.0005	0.4331

filter method applied to the quantised 18 bit encoder. The position as taken from the encoder is differentiated, then filtered with $1st$ order filter with alpha set to $\alpha = 0.1$. The same differentiation method is then applied to the velocity and acceleration terms to gain differentiated estimates of all four states. Figure 7 compares the errors of the joint sensor and the differentiated states. From this the benefit of the extra information from the accelerometers is evident in both the acceleration and velocity terms. Table 2 compares the typical motion RMS error of the differentiated states and sensor states, indicating that better estimates of the position and jerk terms are also available from the sensor.

The effect of deviation in the accelerometer placement in both the IMU and relative component was explored during simulation−2. In this investigation the accelerometers were randomly placed within a cube centred around their specified position, within the SimMechanics simulation. The UKF estimators were only given information about the expected position and were ran ten times for each increasing placement variance. Table 3 shows the results with variance of up to 15mm about the desired placing. This table shows promising results toward the robustness of sensor misplacement within the system.

Simulation−3 examines the sensor performance under extreme dynamic motions. In this simulation damping of the pendulum joints is disabled and the joint torque is set to zero, resulting in highly chaotic motions. The relative link simulation results are shown in Figure 8. This simulation highlights the limitations of the accelerometers under high accelerations. As a result of the device configuration, the accelerometers are limited at $\pm 6g$ (about

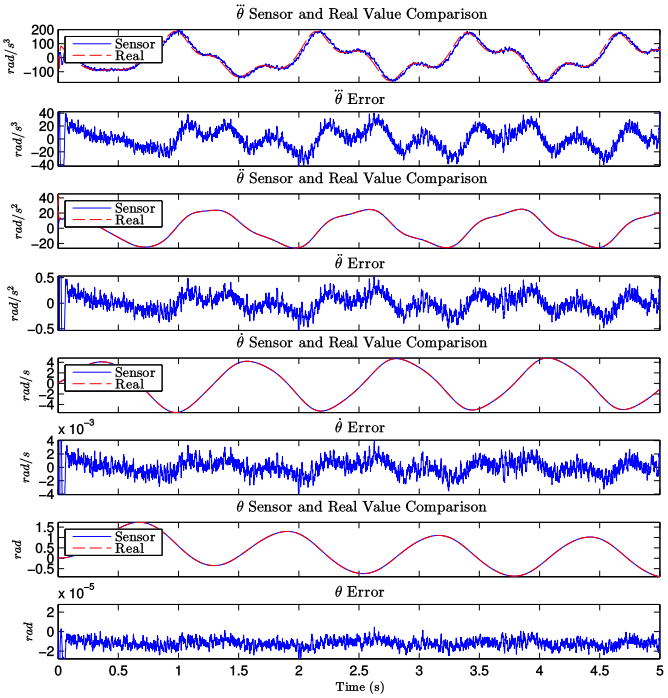

Figure 5: Simulation 2 — Typical Motion: Relative Joint Data.

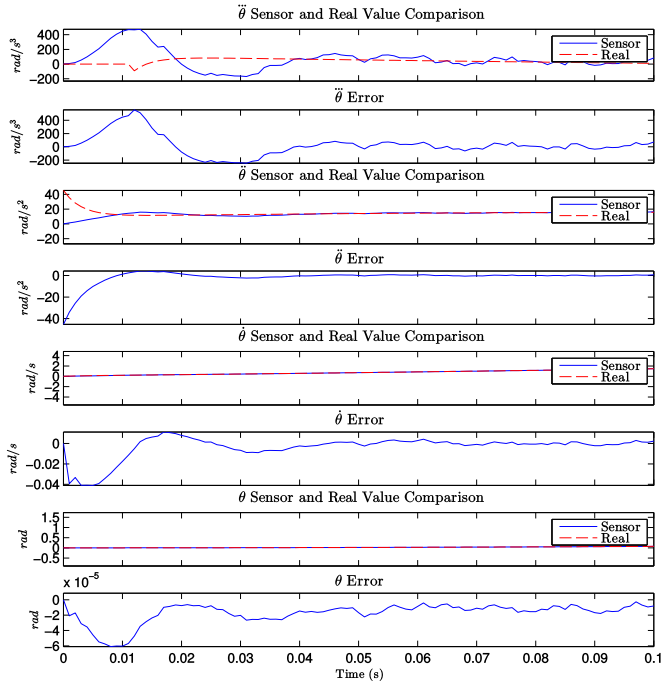

Figure 6: Simulation 2 — Typical Motion: Relative Joint Data Convergence Time.

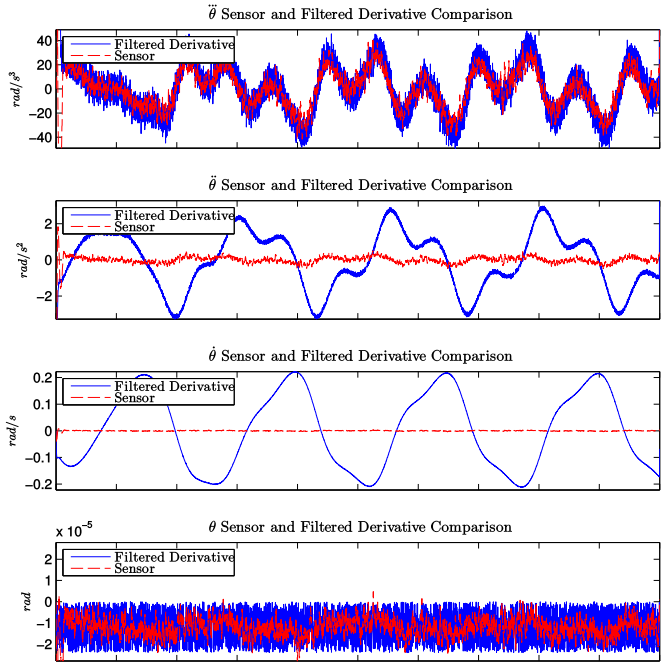

Figure 7: Simulation 2 — Typical Motion: Relative Joint Data Filtered Derivative Comparison.

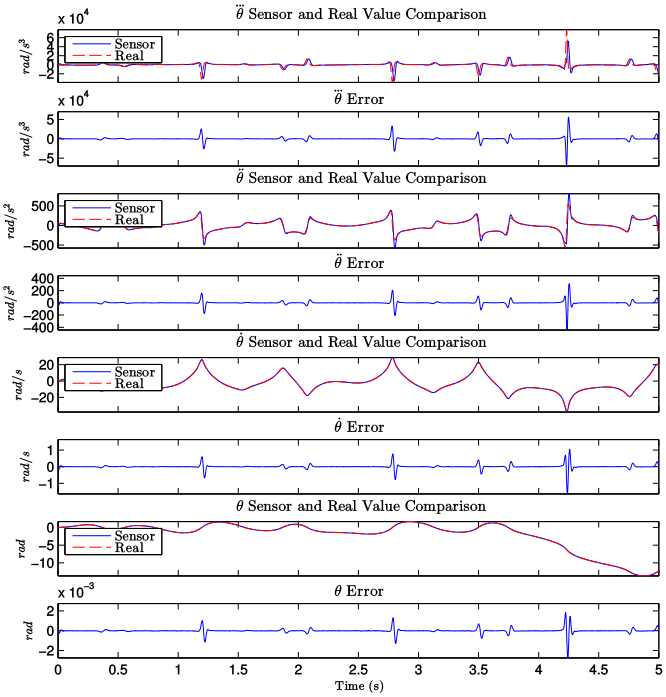

Figure 8: Simulation 3 — Chaotic Motion: Relative Joint Data.

Table 2: Derivative and Joint Sensor RMS Error

		Derivative RMS Err	Sensor RMS Err
$\dddot{\theta}$	$\mathrm{rad\,s^{-3}}$	19.601	15.536
$\ddot{\theta}$	$\mathrm{rad\,s^{-2}}$	1.573	0.1667
$\dot{\theta}$	$\mathrm{rad\,s^{-1}}$	0.1492	1.10×10^{-3}
θ	rad	1.39×10^{-5}	1.29×10^{-5}

Table 3: Accelerometer Placement Error

$\pm$	mm	5	10	15
$\dddot{\theta}$	$\mathrm{rad\,s^{-3}}$	19.0309	26.9387	27.8745
$\ddot{\theta}$	$\mathrm{rad\,s^{-2}}$	0.2430	0.3905	0.4110
$\dot{\theta}$	$\mathrm{rad\,s^{-1}}$	0.0018	0.0030	0.0032
θ	rad	1.35×10^{-5}	1.57×10^{-5}	1.86×10^{-5}

$60\,\mathrm{m/s^2}$) with the result being a saturated acceleration signal as highlighted in Figure 9 at about 4.2 s. The saturated signal propagates through the IMU estimation and becomes apparent in the relative estimation (Figure 8) at the same time, where it significantly affects the relative acceleration estimation. This is also evident in Table 1 with the relative jerk and acceleration components having large RMS errors. Aside from the saturation events, the system still appears to perform well when undergoing highly dynamic motions.

It is clear from the three simulations that the joint sensor system does require some degree of tuning based on the intended application. Table 1 shows that sensor system performed well in both the damped and typical simulations, with no change in the variance required. However variance tuning was required to obtain suitable performance when undergoing the chaotic motions in simulation−3. This is to be expected given the nature of the motions in simulation−3.

5 Future Work

Future work for the joint sensor includes extending the simulation to account for accelerometer bias and off-axis sensitivity and investigating more robust means of process integration. Further simulation testing to explore the performance of the device in three dimensions is also planned. To resolve the acceleration measurement sat-

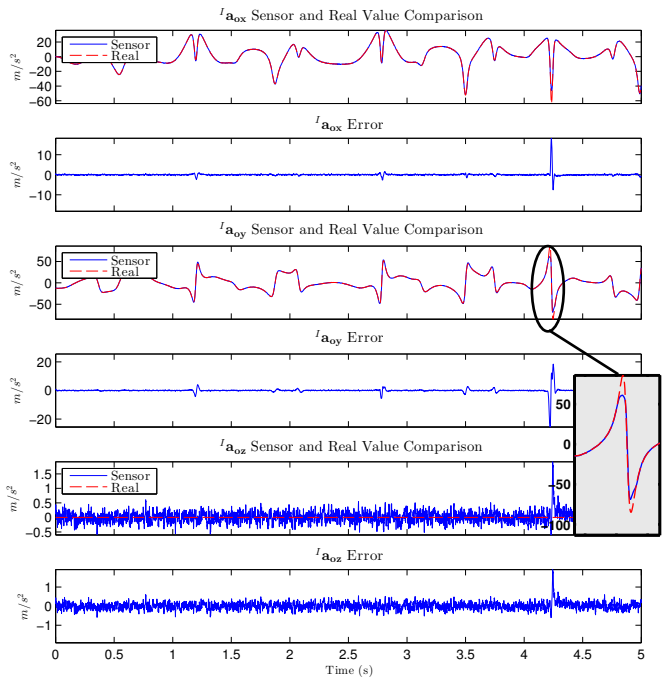

Figure 9: Simulation 3 — Chaotic Motion: Point O Acceleration.

uration issues, an investigation into employing the dynamic sensitivity adjustment available on the accelerometer hardware is of interest, as is the investigation of low resolution encoders to reduce cost. Joint sensor hardware development is planned with an aim to investigate the real world performance and compare the sensor to other joint data estimators.

6 Conclusion

In this work a robotic joint sensor unit has been derived by extending the accelerometer-only IMU formulation to incorporate relative robotic link information. The IMU data were extended and fused with encoder information via the Unscented Kalman Filters to estimate relative angular acceleration, velocity and position and due to the use of the IMU, linear acceleration and angular acceleration and velocity in the inertial frame are also estimated successfully. Simulation of the sensor shows promising results in tracking all states across a range of motions, with some work required in improving inertial frame angular velocity and addressing accelerometer saturation issues.

Acknowledgments

Research undertaken for this paper has been assisted by a grant from the Sir Ross and Sir Keith Smith Fund (Smith Fund) (www.smithfund.org.au). Their support is acknowledged and greatly appreciated.

References

[Schopp *et al.*, 2010] Schopp, Patrick and Klingbeil, Lasse and Peters, Christian and Manoli, Yiannos. *Design, geometry evaluation, and calibration of a gyroscope-free inertial measurement unit.* Elsevier, 2010.

[Lin *et al.*, 2006] Lin, Pei-Chun and Komsuoglu, Haldun and Koditschek, Daniel E. *Sensor data fusion for body state estimation in a hexapod robot with dynamical gaits.* Robotics, IEEE Transactions on, 2006.

[Lu and Lin, 2011] Lu, Jau-Ching and Lin, Pei-Chun. State derivation of a 12-axis gyroscope-free inertial measurement unit. *Sensors*, 2011.

[Wan and Van Der Merwe, 2000] Wan, Eric and Van Der Merwe, Ronell and others. The unscented Kalman filter for nonlinear estimation. *IEEE*, 2000.

[Munoz-Barron *et al.*, 2015] Munoz-Barron, Benigno and Rivera-Guillen, Jesus R and Osornio-Rios, Roque A and Romero-Troncoso, Rene J. *Sensor Fusion for Joint Kinematic Estimation in Serial Robots Using Encoder, Accelerometer and Gyroscope.* Journal of Intelligent & Robotic Systems, 2015.

[Cheng and Oelmann, 2010] Cheng, Peng and Oelmann, Bengt. Joint-angle measurement using accelerometers and gyroscopes A survey. *Instrumentation and Measurement, IEEE Transactions on*, 2010.

[Su *et al.*, 2005] Su, YX and Zheng, CH and Sun, Dong and Duan, Bao Yan. *Sensor Fusion for Joint Kinematic Estimation in Serial Robots Using Encoder, Accelerometer and Gyroscope.* Industrial Electronics, IEEE Transactions on

[Petrella *et al.*, 2007] Petrella, Roberto and Tursini, Marco and Peretti, Luca and Zigliotto, Mauro. *Speed measurement algorithms for low-resolution incremental encoder equipped drives: a comparative analysis.* Electrical Machines and Power Electronics, 2007. ACEMP'07. International Aegean Conference on

[Zhu and Lamarche, 2007] Zhu, Wen-Hong and Lamarche, Tom. Velocity estimation by using position and acceleration sensors. *Industrial Electronics, IEEE Transactions on*, 2007.